Published in final edited form as:
Neurobiol Dis. 2014 June ; 66: 92–103. doi:10.1016/j.nbd.2014.02.012.

Early axonal loss accompanied by impaired endocytosis, abnormal axonal transport, and decreased microtubule stability occur in the model of Krabbe's disease

Carla Andreia Teixeira[a,*], **Catarina Oliveira Miranda**[a,b,*], **Vera Filipe Sousa**[a,b,*], **Telma Emanuela Santos**[a], **Ana Rita Malheiro**[a], **Melani Solomon**[c], **Gustavo H. Maegawa**[c], **Pedro Brites**[a], and **Mónica Mendes Sousa**[a]

[a]Nerve Regeneration Group, IBMC– Instituto de Biologia Molecular e Celular, Rua do Campo Alegre 823, 4150-180 Porto, Portugal

[b]ICBAS – Instituto de Ciências Biomédicas Abel Salazar, Universidade do Porto, Largo Prof. Abel Salazar, 2, 4099-003 Porto, Portugal

[c]McKusick-Nathans Institute of Genetic Medicine & Department of Pediatrics, Johns Hopkins University School of Medicine, Baltimore, MD 21205, USA

Abstract

In Krabbe's Disease (KD), a leukodystrophy caused by β-galactosylceramidase deficiency, demyelination and a myelin-independent axonopathy contribute to the severe neuropathology. Beyond axonopathy, we show that in Twitcher mice, a model of KD, a decreased number of axons both in the PNS and CNS, and of neurons in dorsal root ganglia (DRG), occurred before the onset of demyelination. Despite the early axonal loss, and although *in vitro* Twitcher neurites degenerated over time, Twitcher DRG neurons displayed an initial neurite overgrowth and, following sciatic nerve injury, Twitcher axons were regeneration-competent, at a timepoint where axonopathy was already ongoing. Psychosine, the toxic substrate that accumulates in KD, induced lipid raft clustering. At the mechanistic level, TrkA recruitment to lipid rafts was dysregulated in Twitcher neurons, and defective activation of the ERK1/2 and AKT pathways was identified. Besides defective recruitment of signaling molecules to lipid rafts, the early steps of endocytosis and the transport of endocytic and synaptic vesicles were impaired in Twitcher DRG neurons. Defects in axonal transport, specifically in the retrograde component, correlated with decreased levels of dynein, abnormal levels of post-translational tubulin modifications and decreased microtubule stability. The identification of the axonal defects that precede demyelination in KD, together with the finding that Twitcher axons are regeneration-competent when axonopathy is already installed, open new windows of action to effectively correct the neuropathology that characterizes this disorder.

Corresponding Author: Mónica M Sousa, msousa@ibmc.up.pt, Nerve Regeneration group - IBMC. Rua do Campo Alegre 823, 4150-180 Porto – Portugal; p: +351-22-6074900; fax: +351-22-6099157.
*These authors contributed equally to this work.

Keywords

Krabbe's disease; Twitcher; leukodystrophy; myelin; axonal transport; endocytosis

Introduction

Krabbe's disease (KD) is an autosomal recessive lysosomal storage disorder caused by mutations in β-galactosylceramidase (GALC), an enzyme responsible for the catabolism of myelin galactolipids. The loss-of-function of GALC leads to accumulation of its substrates, galactocerebroside and psychosine (Wenger et al, 1997). Galactocerebroside builds up inside macrophages and microglia giving rise to the globoid cells (Duchen et al, 1980; Jesionek-Kupnicka et al, 1997). Psychosine is considered the main pathological cause of KD (Igisu & Suzuki, 1984), as it disrupts lipid rafts in myelinating glia, culminating in apoptosis of oligodendrocytes and Schwann cells (White et al, 2009; Zaka & Wenger, 2004). As a consequence, demyelination affecting both the central (CNS) and the peripheral nervous system (PNS) is the principal hallmark of KD (Krabbe, 1916; Sabatelli et al, 2002; Sourander & Olsson, 1968). The Twitcher mouse, a model of KD, mimics the most common form of the human disease, which has infantile onset. This naturally occurring model presents a premature stop codon (W339X) in the GALC gene that abolishes enzymatic activity (Lee et al, 2006).

Despite the view that axonopathy in KD is secondary to demyelination, recent evidence supports that axonal defects, not directly caused by loss of myelin, may be a common feature in leukodystrophies, including metachromatic leukodystrophy, Pelizaeus-Merzbacher disease and KD (Castelvetri et al, 2011; Griffiths et al, 1998; Mar & Noetzel, 2010). In KD patients, axonal and neuronal degeneration have been reported sporadically in autopsy material (Sourander & Olsson, 1968). Whether neural degeneration or a dying-back process with Wallerian degeneration takes place in KD nerves has been under discussion for many years (Joosten et al, 1974; Sourander & Olsson, 1968). Recently, psychosine was shown to accumulate not only in myelinating glia, but also in KD neurons (Castelvetri et al, 2011), further supporting a myelin-independent neuronal pathology. In Twitcher mice, axonal swellings and transections occur in sciatic nerves before the onset of myelin loss and progress with age, synchronously with demyelination (Castelvetri et al, 2011; Smith et al, 2011). In these animals, a dying-back neuropathy has been proposed, since apoptosis of motor neurons develops later, while in the sciatic nerve, distal axonal defects are already evident before myelin loss occurs (Castelvetri et al, 2011). Despite the presence of axonopathy, there is still conflicting evidence as to axonal loss in Twitcher nerves (Jacobs et al, 1982; Kobayashi et al, 1988; Tanaka et al, 1988).

The characterization of axonal pathology in KD is still limited, and its understanding is of great interest since therapies devised for this disorder, including enzyme replacement therapy, gene therapy and cell transplantation aim mainly at targeting myelinating cells whereas neuroprotective strategies have been neglected. Currently, the recommended therapy for KD is hematopoietic stem cell transplantation which slows disease progression when performed presymptomatically (Escolar et al, 2005), but fails overtime to address the

complexity of the disorder and to counteract neurologic damage. Here we aimed at clarifying the occurrence of axonal loss in KD and at further characterizing the underlying molecular defects leading to axonopathy in this disorder.

Materials and methods

Animals

Twitcher mice and WT littermates of either sex were obtained from heterozygous breeding pairs (Jackson Laboratory) and genotyped as described (Sakai et al, 1996). All mice were handled according to European legislation. Accessible wet rodent's chow was provided to Twitcher mice after weaning.

Sciatic nerve crush

The sciatic nerve of 3–4 weeks old WT (n=4) and Twitcher mice (n=6), was crushed twice during 15 s using a hemostat (Fine Science Tools). The crush site was maintained constant and identified with a suture in the adjacent muscle. Ten days later, 2 mm portions of the sciatic nerve distal and proximal to the lesion site were collected and processed for morphometric analysis, as described below.

Morphometric analysis

Two mm sciatic nerve segments collected distally from the sciatic notch, dorsal roots and ventral roots, optic and median nerves were isolated at P0, P9 and P30 (according to the setup of each specific experiment) from Twitcher and WT mice, and processed as described (Miranda et al, 2011). One μm thick transverse sections covering the complete cross-sectional area of the nerves or roots were stained with *p*-phenylene-diamine (PPD). For each animal, the total number of myelinated axons in one section was counted. The *g*-ratio was calculated by dividing the diameter of each axon by its myelin-including diameter in over 100 axons per animal. Demyelinated axons were defined as axons with a diameter higher than 1μm that lacked a myelin sheath. To determine the density of unmyelinated axons, ultrathin transverse nerve and root sections (50 nm) were cut and stained with uranyl acetate and lead citrate. For each animal, 15 non-overlapping photomicrographs (6700x magnification) of each section were taken in a transmission electron microscope (JEOL 100CX II). The area of the 15 photomicrographs was determined to calculate the density of unmyelinated axons. In this study, 4 to 6 animals per group were used. The length of the paranodal region was measured in electron micrographs (20000x) of longitudinal sections of median nerves from P9 WT (n=3) and Twitcher (n=3) mice. In all measurements the observer was blind to the genotype and experimental condition.

Quantification of motor neurons and DRG neurons

To quantify motor neurons, the lumbar enlargement of the spinal cord was collected, cut in 4 μm thick serial sections and immunohistochemistry against neurofilament H was performed using a mouse monoclonal antibody (SMI 32, 1:500; Covance). Visualization was done with the avidin-biotin complex (ABC; Vector) using 3-amino-9-ethyl carbazole or 3,3′-diaminobenzidine (Vector) as substrate. The total number of SMI 32-positive motor neurons per section was counted in sections spaced by 28 μm and the average was calculated

(Twitcher mice, n=6; WT littermates, n=4). For the quantification of sensory neurons in Twitcher mice (n=6 at P9 and n=3 at P0) and WT littermates (n=4 at P9 and n=3 at P0), 4 μm thick serial sections were performed of the entire L5 DRG and hematoxylin and eosin staining was performed. The number of sensory neurons was counted in one section every 28 μm in each DRG. Sampling was done in duplicate for each DRG and the average was calculated.

Dorsal root ganglia (DRG) neuron cultures and assessment of neurite outgrowth

Primary sensory neurons were isolated from 3 to 4-weeks-old Twitcher mice and WT littermates as described (Miranda et al, 2011). Dissociated neurons were seeded on poly-L-lysine (PLL)/laminin-coated coverslides in 24-well plates at 7,500 cells/well and maintained in culture for 12 h or up to 7 days in DMEM:F12 supplemented with 50 ng/mL nerve growth factor (NGF), 1% Pen/Strep, 1x B-27 and 2mM of L-glutamine. The DRG culture method described produces a mixture of approximately 20% neurons and 80% glial cells (satellite and Schwann cells). As such, in experiments using DRG cultures, neurons were either identified by β-tubulin III staining, as detailed below, or by the distinctive round morphology of cell bodies, that possess protruding neurites, which contrasts with the spindle-shaped morphology of glial cells and fibroblasts. To analyze neurite outgrowth, fixed DRG neurons were permeabilized in 0.2% Triton X-100 and neurites were visualized using mouse anti-β-tubulin III (1:2,000; Promega) and anti-mouse Alexa Fluor 488 (1:1,000; Molecular Probes). All neurites with a length longer than the cell body diameter were measured using ImageJ/NeuronJ in over 100 neurons/condition. The percentage of neurites with axonal swellings was calculated in WT and Twitcher DRG neuron cultures.

LC-MS/MS quantification of intracellular psychosine levels in cultured DRG neurons

DRG neurons were cultured as above and harvested to produce two cell pellets with an average of 200,000 cells, from two Twitcher and two wild type (WT) mice (one pellet/mouse). Lipid extraction was performed by dispersing cell pellets in 500 μL of HPLC grade methanol containing 9.9 nM 1-acetyl psychosine (purity >98%; Matreya LLC), the internal standard as previously described (Ribbens et al, 2013). Following nitrogen evaporation, lipid film weight was measured using ultra-precision scale. Lipid films were reconstituted with 100 μL of methanol and filtered to remove any residue. The reconstituted lipid solutions were diluted 10 times in HPLC methanol and injected into the QTRAP 5500 Linear Ion Trap Quadrupole LC/MS/MS (Applied Biosystems, SCIEX) coupled with a Waters Acuity UPLC system. Acuity UPLC BEH C8 1.7 μm, 2.1 × 50mm (Waters Inc) column was used. The flow rate was 0.75 mL/min. The samples were analyzed using a gradient elution, which is a modification to the previously reported method (Ribbens et al, 2013). Prior to injection of the sample, the column was equilibrated for 5 minutes with a mixture of 90% mobile phase A (MPA) as water:acetonitrile:formic acid (54.5:45:0.5, v/v/v), and 10% mobile phase B (MPB), comprised of acetonitrile:chloroform:formic acid (90:10:0.5, v/v/v). Both MPA and MPB contained 2mM ammonium formate. Following sample injection, the MPA/MPB ratio was maintained at 90/10 for 0.2 minutes, followed by a linear gradient to 95% MPB over 0.6 minute, and held at 95% MPB for 0.1 minute. Then, a linear gradient back was started to 90% MPA over 0.1 minute, and held at 90% MPA for 0.1 minute. Total run time was 1.1 minute. After, acetonitrile:formic acid (99.5:0.1, v/v/v) and water:acetonitrile (50:50, v/v)

served as the strong wash and weak wash, respectively. Multiple reactions monitoring (MRM) was used to identify the analytes including psychosine (MRM 462/264) and 1-acetyl psychosine (MRM 504/264) as previously described (Ribbens et al, 2013). The integrated areas of the analyte (psychosine) were analyzed using the Analyst® Software, version 1.5.1, (AB SCIEX) and extrapolated in a standard curve of psychosine obtained at concentrations of standard psychosine (Matreya LLC) from 0.025 – 5 ng/mL under exact same conditions. The data is expressed as pmoles of psychosine/mg lipid.

Analysis of microtubule dynamics

DRG neurons from animals at P9 were nucleofected with either pEGFP-EB3 (a kind gift from Dr Jorge Ferreira, IBMC, Porto, Portugal). After transfection, cells were left in suspension for 24h and then plated for 12h in DMEM:F12 supplemented with NGF, Pen/Strep, B27 and L-glutamine. Time-lapse recordings (100 frames every 2 s) were taken on a Spinning Disk (Andor Revolution XD). Kymographs were made using a Matlab script (LAPSO) (Pereira & Maiato, 2010). A minimum of 157 microtubules from at least 18 neurons was quantified.

Analysis of lipid rafts

Lipid rafts were analyzed in WT and Twitcher DRG neurons at two time points, after 16 h or after 5 days in vitro (DIV). For WT DRG neurons, incubated with DMEM:F12 supplemented with NGF, Pen/Strep, B27 and L-glutamine, containing either 10μg/mL of psychosine (Sigma) or vehicle (ethanol), analysis was performed after 5 DIV. In the WT DRG neurons, following an overnight period without drug, psychosine was added to the cells, and medium containing psychosine was changed every two days for the 5 days of incubation. For analysis of lipid rafts, cells were incubated for 15 min with 10 μg/mL cholera toxin B (CTB) (List Biologicals) in ice-cold DMEM:F12 with 1% of FBS at 4°C and then with goat anti-CTB (1:1,000; List Biologicals) for 15 min at 4°C. CTB binds the ganglioside GM1, a constituent of lipid rafts (Chinnapen et al, 2007). Cells were subsequently fixed in formalin, for 15 min at 4°C and 15 min at room temperature, and lipid rafts were visualized with anti-goat Alexa Fluor 568 (Invitrogen; 1:1,000). Cell imaging was done with a Zeiss Axio Imager Z1 microscope and analysis was performed using the deconvolution software, Huygens Professional version 4.1 (Scientific Volume Imaging B.V.). The number, volume and surface area of all lipid rafts per neuron was averaged in at least 30 cells per condition.

Evaluation of endocytosis in Rab5 transduced DRG neurons

DRG neurons from Twitcher and WT mice were transduced with baculovirus expressing a Rab5-GFP transgene using the CellLight® Early Endosomes-GFP, BacMam 2.0 system (Invitrogen). Four thousand DRG neurons were plated in μ-slides ibiTreat (Ibidi) coated with PLL and laminin in DMEM:F12 supplemented with NGF, Pen/Strep, B27 and L-glutamine and 24 h later were exposed to 50 particles of baculovirus/cell for 16 h. Images were acquired using a confocal microscope SP5II (Leica) and the number of endocytic Rab5 positive vesicles per area of neurite was determined using the Fiji software. The vesicle density was determined in at least 30 neurites from each genotype.

Live imaging of axonal transport

DRG neurons (4,000 cells/well) cultured in DMEM:F12 supplemented with NGF, Pen/Strep, B27 and L-glutamine for 16 h in 8-well μ-slides ibiTreat (Ibidi) coated with PLL and laminin were incubated with 100 nM LysoTracker (Invitrogen) in DMEM:F12 for 45 min at 37°C. Lysosomal axonal transport was visualized in a confocal microscope SP5II (Leica) with the cells incubated in supplemented DMEM:F12 without phenol red. Photomicrographs were taken for 2 min with 1sec frame intervals with 5 Z-stacks per frame. For each condition the movement of at least 50 lysosomes was tracked. The velocity of synaptophysin containing vesicles was determined in DRG neurons transduced with CellLight® Synaptophysin-GFP, BacMam 2.0 (Invitrogen). Cells were treated as described for the early endosome labeling and photomicrographs were taken for 2 min with 1sec frame intervals with 5 Z-stacks per frame. For each condition the movement of at least 30 vesicles was tracked. Analysis was done using the Fiji software. Kymographs were designed using the kymograph plug-in of the Fiji software.

Analysis of the TrkA content in lipid rafts and in early endosomes

After 4 DIV in DMEM:F12 supplemented with NGF, Pen/Strep, B27 and L-glutamine, DRG neurons from Twitcher and WT littermates were grown for 16 h in the same media without NGF after which cells were incubated at 37°C for 5 min in DMEM:F12 with or without 100 ng/mL of NGF. After NGF stimulation, labeling with CTB was performed as described above, followed by immunolabeling with rabbit anti-TrkA (1:100, Santa Cruz Biotechnology) overnight at 4°C. Cell imaging was done with a confocal microscope SP5II (Leica) and analysis was performed with the deconvolution software, Huygens Professional version 4.1 using the optimized threshold and Manders coefficient for the co-localization measurements. Results are expressed as the ratio of co-localization of TrkA (red) in lipid rafts (green). For the co-localization of TrkA in the Rab5 positive endocytic vesicles, DRG neurons transduced with CellLight® Early Endosomes-GFP BacMam 2.0 were fixed with 2% paraformaldehyde and immunolabeled with rabbit anti-TrkA (1:100, Santa Cruz biotechnology). Images acquired with a Zeiss Axio Imager Z1 microscope were analyzed using the Fiji software. The percentage of early endosomes positive for TrkA was averaged in at least 30 cells per condition.

Analysis of TrkA phosphorylation

After 4 DIV in DMEM:F12 supplemented with NGF, Pen/Strep, B27 and L-glutamine, DRG neurons from Twitcher and WT littermates were grown for 16 h in the same media without NGF after which cells were incubated at 37°C for 20 min in DMEM:F12 with or without 100 ng/mL NGF. After NGF stimulation, cells were fixed in 2% PFA for 20 min at room temperature, followed by immunolabeling with rabbit anti-pTrkA (1:10, Abcam) and mouse anti-β-tubulin III (1:2,000, Promega). Images acquired with a Zeiss Axio Imager Z1 microscope were analyzed using the Fiji software. The ratio of pTrkA positive particles and the cell body area was calculated in at least 20 cells per condition.

Western blotting

DRG neurons from WT (n=4) and Twitcher (n=5) mice with 3–4 weeks of age were dissociated as described above. Dissociated DRG neurons were incubated in DMEM:F12 with or without 100 ng/mL of NGF for 20 min at 37°C. The cell pellets were stored at −20°C until use. Sciatic nerves from WT (n=6) and Twitcher (n=7) mice at P9 were homogenized in lysis buffer (PBS with 0.1% Triton X-100, 1mM sodium orthovanadate and protease inhibitor cocktail from General Electric). In all samples, total protein was determined with Bio-Rad DC kit. Protein lysates were run on 12% SDS-PAGE (20μg/lane) and transferred to nitrocellulose membranes (Amersham). Membranes were incubated overnight at 4°C with the primary antibodies: rabbit anti-phospho-ERK1/2 (1:1,000; Cell Signaling), rabbit anti-ERK1/2 (1:1,000; Cell Signaling), rabbit anti-phospho-AKT (1:2,000; Cell Signaling), rabbit anti-AKT (1:1,000; Cell Signaling), rabbit anti-phospho-MEK1/2 (1:1,000; Cell Signaling), rabbit anti-phospho-PDK1 (1:1,000; Cell Signaling), mouse anti-kinesin-1 heavy chain (1: 5,000; Millipore), mouse anti-cytoplasmic dynein 1 intermediate chain 1 (1:250; Millipore), mouse anti-acetylated tubulin (1:5,000; Sigma), rabbit anti-histone deacetylase 6, HDAC6 (1:500; Cell signaling), mouse anti-polyglutamylated tubulin (1:4,000; AdipoGen), mouse anti-α tubulin (1:1,000; Sigma), mouse anti-β-actin (1:2,500; Sigma) and with the secondary antibodies anti-rabbit or anti-mouse HRP (1:5,000; Jackson Immunoresearch). Proteins were detected using ECL (Thermo Scientific). For each experiment, representative western blots are shown. Densitometry was performed with QuantityOne software (Bio-Rad).

Reverse Transcriptase-Polymerase Chain Reaction

Total RNA extraction was performed with Trizol (Invitrogen) and reverse transcription with the Superscript II kit (Invitrogen) using oligo-dT. Expression in DRG neurons of TrkA, cytoplasmic dynein 1 intermediate chain 1 (Dnai1) and kinesin-1 heavy chain (Kif5b) was analyzed by qPCR performed with the iQTM SybrGreen Supermix kit (Bio-Rad Laboratories, Lda) at 94 °C for 3 minutes and 94 °C for 15 s, 59 °C for 20 s, and 72 °C for 15 s, 40 cycles. β-actin expression was used for normalization, and the Livak method was used for quantifications. Specific primers, designed with Beacon software, were as follows: TrkA (NM_001033124.1): 5′-ACGGAGCTCTACGTGGAAAA-3′ and 5′-GAACAGGGCACAGGAACAAT-3′; Kif5b (Gene ID 16573): 5′-GCAGGAACGGCTAAGGGTGGAG - 3′ and 5′-CCGCCAGTGTCGTCAGAGTCG - 3′ and Dnai1 (Gene ID 68922): 5′-AGGGACTGATGTGGGAGAAGG-3′ and 5′-TGTGGGTTGTTTGCTGTCAGG- 3′.

Statistical analysis

Results are presented as mean ± SEM. Mann-Whitney U test was used to compare the *g*-ratio measurements. In all other analyses the Student's *t*-test or one-way ANOVA (for multiple comparisons) were performed. $P<0.05$ was considered statistically significant. *$P<0.05$, **$P<0.01$, ***$P<0.001$.

Results

In Twitcher nerves, a decrease in axon number precedes demyelination

Given the conflicting evidence related to axonal loss in Twitcher nerves, and to establish whether besides axonopathy, a decreased axon number occurs prior to demyelination, we performed a comprehensive evaluation of nerve pathology in this animal model. In peripheral nerves from Twitcher mice, demyelination initiates around P15 (Smith et al, 2011) with a clear decrease in myelin thickness starting only around P20 (Tanaka et al, 1988). Our analysis showed that sciatic nerves from P9 Twitcher mice lacked signs of demyelination (Fig. 1A). At P9, g-ratio analysis did not reveal differences in myelin thickness between WT and Twitcher sciatic nerves (Fig. 1B). Besides, measurement of paranodal regions in longitudinal sections of nerves from WT and Twitcher mice were also similar (WT 2.76μm ± 0.06 vs. twi 2.73μm ± 0.04; p=0.226). However, at P30, nerves from Twitcher mice showed clear signs of demyelination with reduced myelin thickness (Fig. 1A) and a significant increase of the g-ratio (Fig. 1B). Despite the absence of demyelination at P9, a 1.4-fold decrease in the total number of myelinated axons was already observed in Twitcher sciatic nerves (Fig. 1C). No defect in axonal radial growth was detected at P9, as the distribution of myelinated axons by their axonal diameter did not differ between Twitcher and WT mice (Fig. 1D), despite the described decrease in radial growth during the demyelinating period (Cantuti-Castelvetri et al, 2012). At P9, no endoneurial edema was evident, as there were no differences in the cross-sectional areas of the sciatic nerves of the two genotypes (0.063 ± 0.005 mm^2 and 0.057 ± 0.002 mm^2, WT and Twitcher mice, respectively; p=0.34). These data support that the decreased number of myelinated axons at P9 is caused by a defect unrelated to demyelination. At P30, when overt demyelination occurs, there was a 1.5-fold decrease in the total number of myelinated axons in Twitcher mice, relatively to WT mice (Fig. 1C). At birth (P0), the densities of myelinated (Fig. 1E) and unmyelinated (Fig. 1F) axons were similar in WT and Twitcher sciatic nerves, indicating that the observed defects at P9 were not caused by a developmental impairment in Twitcher mice.

To understand whether the sciatic nerve axonopathy had a differential contribution of sensory and motor axons, we determined the density of myelinated axons in the dorsal and ventral roots of WT and Twitcher mouse littermates at P9 and P30. Axon densities are presented as no differences in cross-sectional root areas were found between genotypes. At P9, before the onset of demyelination, a decreased density of myelinated axons in the dorsal and ventral roots of Twitcher mice was already detected (Fig. 1G, H). Sensory and motor axons were similarly affected at P9 (1.2 and 1.3-fold decreased density in Twitcher dorsal and ventral roots, respectively) and at P30 (2.5 and 3.0-fold decreased density in Twitcher dorsal and ventral roots, respectively). The progressive loss of myelinated fibers from P9 to P30 in spinal roots of Twitcher mice (Fig. 1G, H) is likely due to the combination of the gradually developing myelin-independent axonopathy and of axonal loss as a secondary effect of demyelination. In addition, whereas at P0 we did not observe a difference in the number of sensory neurons (p=0.377), at P9, a 1.4-fold decrease in the number of sensory neurons (p=0.03) was found in Twitcher mice (Fig. 1I). However, the number of motor neurons remained unaffected (Fig. 1J). As such, at least for some neuronal populations,

neuronal loss occurs as an early event, preceding demyelination. As dysmyelination could also contribute to the decreased number of myelinated axons in Twitcher sciatic nerves at P9, the density of unmyelinated axons, i.e., the density of axons with a diameter smaller than 1μm, was determined. In Twitcher mice, unmyelinated axon density was 1.4-fold decreased at P9 further confirming that the decrease in axonal number precedes, and is unrelated to myelination or demyelination (p=0.04) (Fig. 1K, L).

To determine whether our findings might be restricted to the sciatic nerve, the median nerve was also analyzed. Similarly to the sciatic nerve, no differences were found at P0 in the densities of myelinated and unmyelinated axons in the median nerve of Twitcher mice (data not shown). However, at P9 a 1.4-fold (p=0.015) and 1.3-fold (p<0.001) decrease in the density of myelinated (Fig. 2A, B) and unmyelinated axons (Fig. 2C, D), respectively, was found. No differences in the areas of the median nerve between genotypes were found (p=0.486), allowing for the comparison of axonal densities. These observations were not restricted to the PNS but extended to the optic nerves of Twitcher mice. At P0.5, the density of axons was similar between WT and Twitcher optic nerves (Fig. 2E). At P9, the Twitcher optic nerves presented a decreased density of myelinated and unmyelinated axons (1.9-fold, p=0.014 and 8.1-fold, p=0.0003, respectively) (Fig. 2E, F). At this time point no edema was present as there were no differences in the area of the optic nerves of Twitcher and WT mice (0.0307 ± 0.0050 mm^2 in twi vs 0.0308 ± 0.0067 mm^2 in WT; p=0.489). Combined, these data indicate that the reduced number of axons observed at P9 is not the result of a developmental defect, but rather of the degeneration and loss of axons. Thus, we provide quantitative evidence that in the Twitcher nerves, axonal loss is an early event that precedes demyelination.

Twitcher axons are regeneration-competent and Twitcher Schwann cells are capable of remyelination

To further explore the axonal pathology of Twitcher mice, the neurite outgrowth of Twitcher DRG neurons was assessed *in vitro*. Unexpectedly, after 12h in culture, Twitcher DRG neurons had a 1.6 fold increase in neurite outgrowth when compared to WT DRG neurons (p=0.02; Fig. 3A). However, at 5DIV, axonal swellings were evident, whereas this feature was rare in WT DRG neurons (p<0.0001; Fig. 3B, D). After 7 DIV, Twitcher DRG neurons had a decreased percentage of cells with neurites when compared to WT neurons (p<0.0001; Fig. 3C, D). This data suggests that the initial neurite overgrowth of Twitcher neurons fails overtime, and is surpassed by neurite degeneration.

Axonal regeneration following nerve injury is a paradigm extensively used to evaluate not only axonal growth but also the existence of axonal pathology. As such, sciatic nerve crush was performed in WT and Twitcher mice at P24 and axonal growth was evaluated 10 days after injury. After a PNS lesion, the distal axonal segment undergoes degeneration, while the proximal segment regenerates such that around eight days after injury, Schwann cells contact with regenerating axons and start to remyelinate (Akassoglou et al, 2002; Fawcett & Keynes, 1990). Interestingly, Twitcher axons did not show any intrinsic incapacity to regenerate after injury. Ten days after injury, in sciatic nerves from Twitcher mice distal to the injury site, not only axonal growth but also remyelination occurred such that myelinated

axons could be clearly observed (Fig. 3E). Moreover, no differences in *g*-ratio were found between WT and twi (p=1.00) (Fig. 3F, G) further showing that even when injury is performed during the active demyelination stages, Twitcher Schwann cells are still capable of remyelinating.

In Twitcher mice, the number of myelinated axons distally to the injury site was 1.4-fold decreased when compared to WT animals (SN dist, p=0.03) but a similar decrease (1.6-fold) was found between the two strains proximally to the injury site (SN prox, p=0.01) (Fig. 3H). This data supports that the decreased number of axons distally to the injury may not reflect impairment in regeneration but only the primary axonal defect that existed before injury (i.e., the decreased total number of myelinated axons proximally to the lesion site). Both in WT and in Twitcher mice, no significant neuronal loss occurred post-injury, as can be observed when comparing the number of myelinated axons proximally to the injury site (SN prox, Fig. 3H) with that of control age-matched Twitcher sciatic nerves (control, Fig. 3H) (WT: p=0.40; twi: p=0.95). However, in Twitcher mice, regenerating myelinated axons had an overall smaller caliber than WT axons (Fig. 3I), that can be accounted by dephosphorylation of neurofilaments (Cantuti-Castelvetri et al, 2012). Overall our results indicate that in Twitcher nerves axonal regeneration may occur despite intrinsic axonal defects.

Psychosine accumulation in neurons causes lipid raft clustering

In the brain of KD patients, accumulation of psychosine in lipid rafts is accompanied by an increase in cholesterol and by changes in the distribution of caveolin-1 and flotilin-2 that have been suggested to induce the disruption of the raft architecture (White et al, 2009). To further characterize this alteration, we compared the integrity of lipid rafts in WT and Twitcher DRG neurons. In Twitcher DRG neuron cultures, psychosine accumulated, as expected (WT neurons 0.18± 0.02, Twitcher neurons 2.44± 0.35 pmol psychosine/mg lipid). After 16 h in culture, Twitcher DRG neurons had an increased number of lipid rafts (p<0.0001) (Fig. 4A), but after 5 DIV the number of lipid rafts in Twitcher DRG neurons decreased relatively to WT DRG neurons (p=0.0174) that retained a constant number of rafts throughout this period (Fig. 4A, D). Despite the increased number of lipid rafts after 16 h in culture, there were no major differences in their volume (p=0.72) (Fig. 4B) or surface area (Fig. 4C) when compared to WT DRG neurons (p=0.094). However, following 5 DIV, Twitcher lipid rafts presented a 2.2- fold increased volume (p=0.0049) (Fig. 4B, D) and a 1.5-fold increase in surface area (p=0.033) (Fig. 4C, D). To address if these changes were caused directly by psychosine, WT DRG neurons were incubated with psychosine for 5 DIV and lipid rafts were analyzed. Although no significant differences were found in the number of lipid rafts, psychosine led to a 9.9-fold increase in the volume (p=0.0093) (Fig. 4E, F) and a 6.2-fold increase in surface area (p=0.0025) (Fig. 4E, F) of lipid rafts. Together these data suggest that psychosine accumulation causes lipid raft clustering in Twitcher neurons.

Regulation of TrkA recruitment to lipid rafts and TrkA-mediated signal transduction are impaired in Twitcher DRG neurons

In neurons, lipid rafts are important for signal transduction as they act as platforms where specific proteins localize and interact with other proteins or lipids to initiate signaling

events, such as those mediated by neurotrophic factors (Tsui-Pierchala et al, 2002). Tyrosine kinase receptors, such as TrkA, move into lipid rafts upon activation along with their effectors to initiate multiple intracellular signaling cascades (Pryor et al, 2012). In Twitcher neurons, at baseline, there was an increased recruitment of TrkA to lipid rafts, when compared to WT neurons (Fig. 5A, B). In WT DRG neurons, following NGF stimulation, TrkA was recruited to lipid rafts (Fig. 5A, B). Of note, in Twitcher DRG neurons, the basal level of TrkA localization in lipid rafts was similar to that of stimulated WT DRG neurons (p=0.49) (Fig. 5A, B). Moreover, following NGF stimulation there were no differences between WT and Twitcher neurons. Upon NGF stimulation there was an increase in TrkA phosphorylation in WT DRG neurons (Fig. 5C). However, the basal levels of phosphorylated TrkA were increased in Twitcher DRG neurons, but stimulation with NGF failed to elicit further phosphorylation of TrkA (Fig. 5C). These data suggests that in Twitcher neurons TrkA might be constitutively recruited to lipid rafts as a consequence of their altered architecture, but activation upon stimulus is impaired. To further assess whether the TrkA-mediated signal transduction was affected in Twitcher neurons, the downstream pathways Raf–MEK–ERK and PI3K–PDK1–AKT were evaluated. In Twitcher DRG neurons, a 9.8-fold decrease in MEK1/2 activation (p=0.002) was observed (Fig. 5D, E). Accordingly, there was a 2.0-fold decrease in the amount of phosphorylated ERK1/2 in Twitcher DRG neurons (p=0.008) (Fig. 5D, E). Moreover, in the presence of NGF, the levels of phosphorylated ERK1/2 were increased both in WT and Twitcher DRG neurons when compared to the respective basal conditions (Fig. 5F). However, phosphorylated ERK1/2 in NGF-activated Twitcher neurons did not reach the levels observed in NGF-activated WT neurons (Fig. 5F). In the PI3K pathway, the downstream effectors PDK1 and AKT were also less phosphorylated in Twitcher DRG neurons when compared to WT DRG neurons (6.8-fold, p=0.035 and 9.9-fold, p=0.013, respectively) (Fig. 5D, E). As DRG neurons are isolated together with satellite cells and Schwann cells, one cannot rule out that glial cells may also contribute to the effects observed on western blot analyses.

Together, this data shows that TrkA recruitment to lipid rafts and activation of the ERK1/2 and AKT pathways are impaired in Twitcher neurons. Although the impairment in the activation of the ERK1/2 and AKT pathways might result from the abnormal TrkA recruitment to lipid rafts, one cannot exclude additional causes for the decreased phosphorylation of these signaling molecules.

The early steps of endocytosis and the transport of endocytic and synaptic vesicles are impaired in the Twitcher DRG neurons

To further dissect the defective Trk signaling in Twitcher neurons, endocytosis and axonal transport of endocytic vesicles were evaluated. When a neurotrophin binds to Trk receptors, given the polarized nature of neurons, the ligand-Trk receptor complex recruits the machinery responsible for endocytosis and is internalized in a lipid raft-dependent manner forming a signaling endosome, that traffics retrogradely to the cell body (Delcroix et al, 2003; Zweifel et al, 2005). In Twitcher DRG neurons transduced with Rab5-GFP, a marker of early endosomes that is retained in Trk signaling endosomes (Delcroix et al, 2003), a 2.5-fold decreased density of $Rab5^+$ vesicles was observed (p=0.003) (Fig. 6A). Moreover, the percentage of $Rab5^+$ vesicles containing TrkA was 1.4-fold decreased in Twitcher DRG

neurons (p=0.04) (Fig. 6B), further suggesting that the endocytic pathway, specifically the formation of Trk signaling endosomes is impaired. Of note, TrkA mRNA expression was not altered in Twitcher DRG neurons (Fig. 6C).

Due to the characteristic Brownian-like motion of endosomes, we assessed the transport of an alternative type of vesicle of the endocytic pathway, the lysosomes. The velocity of retrogradely transported lysosomes was 1.3-fold decreased in Twitcher DRG neurons (p=0.006) (Fig 6D). No differences were found in the anterograde transport velocity (p=0.65) (Fig. 6D). A decreased percentage of vesicles that moved in the retrograde direction and a trend for an increased percentage of stationary vesicles were observed in Twitcher DRG neurons (Fig. 6E, G). Interestingly, a 1.3-fold decrease in lysosomal density was found in Twitcher DRG neurites (p=0.0023) (Fig. 6F). This data further reinforces the presence of defects in the endocytic pathway. To further determine whether the defect in axonal transport could be extended to synaptic vesicles, we analyzed the transport of synaptophysin following transduction of WT and Twitcher DRG neurons. A 1.5-fold decrease in retrograde transport velocity of synaptophysin positive vesicles was found in Twitcher DRG neurons (p=0.02) and similarly to what was observed with lysosomes, no differences were found in the anterograde component of axonal transport (p=0.59) (Fig. 6H, I). Overall our data shows that the early steps of endocytosis and the retrograde transport of endocytic and synaptic vesicles are defective in Twitcher neurons.

The axonal transport impairment in Twitcher neurons is related to decreased levels of dynein and decreased microtubule stability

To better understand the molecular details underlying the defects in axonal transport, we analyzed the expression of both kinesin-1 heavy chain and cytoplasmic dynein 1, the molecular motors for anterograde and retrograde transport, respectively. Kinesin-1 (KIF5 or conventional kinesin) is the motor that transports a broader range of cargo types including mitochondria, lysosomes, synaptic vesicles precursors and Rab5 containing endosomes (Hirokawa et al, 2009). At the mRNA level, no significant changes were observed in kinesin expression, whereas dynein was 1.5-fold decreased (p=0.03) in P9 DRG from Twitcher mice (Fig. 7A), correlating well with the observed specific defect in the retrograde component of axonal transport. At the protein level, in the sciatic nerve of Twitcher mice at P9, similar findings were observed with no significant variation in kinesin levels and a 1.6-fold decrease in dynein (p=0.03, Fig. 7B, C) which may account, at least in part, for defects in retrograde axonal transport.

As the interaction between microtubules and motor proteins is regulated by post-translational modifications of tubulin, putative changes in these modifications, that might underlie defects in axonal transport, were investigated. Cytoplasmic dynein and kinesin-1 bind more effectively to polyglutamylated (Ikegami et al, 2007) and acetylated (Dompierre et al, 2007; Reed et al, 2006) microtubules. In the sciatic nerve of P9 Twitcher mice, a 2.1-fold decrease (p=0.042) in polyglutamylated tubulin and a 1.8-fold decrease (p=0.009) in acetylated tubulin were found (Fig. 7D, E). The protein levels of HDAC6, the histone deacetylase that catalyzes α-tubulin deacetylation (Matsuyama et al, 2002), were unchanged (Fig. 7D, E), indicating that decreased acetylated α-tubulin levels are independent of

HDAC6. Besides regulating binding of motors, both tubulin acetylation and polyglutamylation are generally seen as tubulin modifications that characterize stable microtubules (Janke & Bulinski, 2011). As such, their decreased levels in Twitcher nerves suggest decreased microtubule stability. At the plus-end, microtubules undergo rapid switches from growth to shrinkage (catastrophe) and from shrinkage to growth (rescue), a behavior termed dynamic instability (Howard & Hyman, 2003). Following transfection with the plus-tip binding protein EB3, we show that Twitcher neurons have an increased microtubule growth speed (Fig. 7F), which suggests a higher dynamic state of the growth cone. In summary, Twitcher neurons have a generalized impairment in axonal transport that may result from decreased dynein levels and defects in microtubule post-translational modifications and stability.

Discussion

In KD, axonal damage and loss are generally seen as a consequence of the progressive demyelination. Our work shows that however, before the onset of demyelination, the number of both myelinated and unmyelinated axons is already decreased in Twitcher mice. Neuronal defects, resulting from the combined or synergistic contribution of psychosine-induced lipid raft clustering, impaired endocytosis, decreased microtubule stability and defective axonal transport, may originate abnormal signaling and axonal loss (Fig. 8). Several recent reports demonstrate that endocytosis and axonal transport are cellular processes that need to be tuned in synergy to enable proper cell function. In this context, it has been demonstrated that NGF causes TrkA to specifically attract microtubules to lipid rafts and that this mechanism is important for endocytosis, signal transduction and axon growth (Pryor et al, 2012). Besides, activation of the ERK1/2 pathway by Trk enhances dynein binding to signaling endosomes for retrograde axonal transport (Mitchell et al, 2012). In Krabbe's disease, GALC deficiency is accompanied by psychosine accumulation in lipid rafts and this effect may lead to the dysregulation of the attraction of microtubules to these membrane microdomains, thereby affecting their dynamics. The mechanisms underlying the differences observed at the level of expression of molecular motors and posttranslational tubulin modifications remain to be further dissected.

Consistent with our data, reports of loss of unmyelinated axons exist in KD. Sural nerve biopsies of two patients with adult-onset KD revealed either a decreased number or a total absence of unmyelinated axons (Sourander & Olsson, 1968). In one of the patients, although electrophysiological examination was consistent with a demyelinating neuropathy, axonal loss was suggested to be the cause of the electrophysiological findings. Overlooked from the perspective of a leukodystrophy, and combined with scarce and inconsistent information, axonal damage and loss preceding the active demyelinating stage of the disease, should also be regarded as a primary defect and as a target in the design of therapeutic approaches. In this respect, delivery of mesenchymal stromal cells has been shown to rescue and effectively improve the neuropathology of myelinated and unmyelinated axons, respectively, in sciatic nerves from Twitcher mice (Miranda et al, 2011; Miranda et al, 2013). Here, we also show that Twitcher axons are regeneration-competent, even in a stage of overt demyelination. We also demonstrate that following sciatic nerve crush, Twitcher Schwann cells were capable of remyelinating normally despite that demyelination was installed. The observation that no

impaired axon regeneration is detected in Twitcher nerves despite that major signal transduction pathways related to growth are strongly suppressed in Twitcher cells is puzzling. However, these findings open the prospect that a wider temporal therapeutic window of opportunity may exist to effectively correct the neuropathology that characterizes KD which is particularly relevant in this disorder as usually diagnosis happens after clinical symptoms appear.

To further understand the neuronal pathology of KD, we identified several factors that can operate synergistically to contribute to axonal loss in Twitcher nerves (Fig. 8). The lipid raft clustering induced by psychosine can promote physical alterations in the membrane (Simons & Gruenberg, 2000) (Fig. 8A) that abrogate correct endosome formation (Fig. 8B) and signaling (Fig. 8C). In fact, supporting the clinical relevance of our findings, abnormal membrane trafficking along the endocytic pathway has been described in KD fibroblasts (Pagano et al, 2000). In these cells, raft-mediated endocytosis and intracellular sorting of glycosphingolipids was altered leading to glycosphingolipid accumulation in the lysosome. In addition, we show that one key cellular pathway affected by the altered lipid raft architecture is neurotrophin signaling, although most probably, defects in other signaling cascades triggered by molecules present within lipid rafts may exist in KD. Although in Twitcher DRG neurons an increased basal location of TrkA in lipid rafts was found, this did not correlate with a normal or increased signal transduction, most probably given the downstream defects in endocytosis and axonal transport. In mouse oligodendrocyte progenitor cells, the inhibitory effect of psychosine in the phosphorylation of AKT and ERK 1/2 has also been demonstrated (Zaka et al, 2005). In this report, insulin-like growth factor-1 (IGF-1) provided protection from psychosine-induced cell death by sustaining the phosphorylation of AKT and ERK, which are the main anti-apoptotic pathways of the IGF-1 receptor. Our data opens the possibility that IGF-1-associated therapies might also be relevant in counteracting the axonopathy in KD.

Psychosine has been recently shown to inhibit axonal transport of mitochondria (both in the retrograde and anterograde direction) by activation of GSK3β and deregulation of kinesin light chain (Cantuti Castelvetri et al, 2013). The decreased levels of phosphorylated AKT here reported may underlie the decreased phosphorylation of its substrate, GSK3β at serine 9, that was described in sciatic nerves from Twitcher mice (Cantuti Castelvetri et al, 2013). In that report, the GSK3β pathway has been primarily associated with the regulation of anterograde transport (Cantuti Castelvetri et al, 2013), but we now show important defects specifically in the retrograde component of axonal transport that are probably not accounted by defects in GSK3β signaling. Besides, despite the deregulation shown in kinesin light chain in Twitcher mice (Cantuti Castelvetri et al, 2013), we show that the anterograde transport of synaptophysin and lysosomes is unaffected in mutant neurons. In accordance with previous data reporting that recovery of transport using PP1/GSK3β inhibitors was not complete (Cantuti Castelvetri et al, 2013), we provide additional mechanisms that are probably involved in the impaired axonal transport in KD, namely the decreased levels of dynein and of acetylated and polyglutamylated tubulin. In recent years, many studies have focused on HDAC6, a tubulin deacetylase, as a target for therapy in neurodegenerative diseases and in injury conditions where axonal transport is affected as a consequence of decreased tubulin acetylation (Chen et al, 2010; Dompierre et al, 2007; Rivieccio et al,

2009). However in Twitcher neurons, the levels of HDAC6 were normal, suggesting that decreased tubulin acetylation is accounted by a HDAC6-independent mechanism, and raising uncertainty as for the therapeutic benefit of using HDAC6 inhibitors in KD. Several studies have shown that using low concentrations of microtubule stabilizing drugs enhances the axonal growth capacity and decreases axonal degeneration (Erturk et al, 2007; Hellal et al, 2011). In this context, and given that we show that Twitcher axons are characterized by decreased microtubule stability, the use of microtubule stabilizing drugs such as taxol might be a beneficial therapeutic approach.

In conclusion, our data show that independently of demyelination, a decreased number of axons characterizes the early stages of KD pathology. Hence, the recognition of an axonal defect that precedes the death of myelinating glia in KD opens new windows of action to effectively correct the neuropathology of this disorder, which may include IGF-1 and neurotrophin-related therapies, and microtubule-stabilizing drugs.

Acknowledgments

This work was funded by the European Leukodystrophy Association to M.M.S. and P.B. (ELA 2010-042C5) and by FEDER funds through the Operational Competitiveness Programme – COMPETE and by National Funds through FCT – Fundação para a Ciência e a Tecnologia under projects PTDC/SAU-ORG/112406/2009 (to P.B.) and PTDC/SAU-GMG/111761/2009 (to M.M.S). C.O.M. was funded by Fundação para a Ciência e Tecnologia (SFRH/BD/29768/2006), C.A.T. was supported by Programa Ciência, funded by POPH-QREN and MCTES. P.B is an Investigator FCT. The authors declare no competing financial interests. The authors would like to thank Catarina Silva (IBMC) for the help in quantifying the co-localization of TrkA in endosomes and axonal transport of synaptophysin.

References

Akassoglou K, Yu WM, Akpinar P, Strickland S. Fibrin inhibits peripheral nerve remyelination by regulating Schwann cell differentiation. Neuron. 2002; 33:861–875. [PubMed: 11906694]

Cantuti Castelvetri L, Givogri MI, Hebert A, Smith B, Song Y, Kaminska A, Lopez-Rosas A, Morfini G, Pigino G, Sands M, Brady ST, Bongarzone ER. The Sphingolipid Psychosine Inhibits Fast Axonal Transport in Krabbe Disease by Activation of GSK3beta and Deregulation of Molecular Motors. J Neurosci. 2013; 33:10048–10056. [PubMed: 23761900]

Cantuti-Castelvetri L, Zhu H, Givogri MI, Chidavaenzi RL, Lopez-Rosas A, Bongarzone ER. Psychosine induces the dephosphorylation of neurofilaments by deregulation of PP1 and PP2A phosphatases. Neurobiol Dis. 2012; 46:325–335. [PubMed: 22326830]

Castelvetri LC, Givogri MI, Zhu H, Smith B, Lopez-Rosas A, Qiu X, van Breemen R, Bongarzone ER. Axonopathy is a compounding factor in the pathogenesis of Krabbe disease. Acta Neuropathol. 2011; 122:35–48. [PubMed: 21373782]

Chen S, Owens GC, Makarenkova H, Edelman DB. HDAC6 regulates mitochondrial transport in hippocampal neurons. PLoS One. 2010; 5:e10848. [PubMed: 20520769]

Chinnapen DJ, Chinnapen H, Saslowsky D, Lencer WI. Rafting with cholera toxin: endocytosis and trafficking from plasma membrane to ER. FEMS Microbiol Lett. 2007; 266:129–137. [PubMed: 17156122]

Delcroix JD, Valletta JS, Wu C, Hunt SJ, Kowal AS, Mobley WC. NGF signaling in sensory neurons: evidence that early endosomes carry NGF retrograde signals. Neuron. 2003; 39:69–84. [PubMed: 12848933]

Dompierre JP, Godin JD, Charrin BC, Cordelieres FP, King SJ, Humbert S, Saudou F. Histone deacetylase 6 inhibition compensates for the transport deficit in Huntington's disease by increasing tubulin acetylation. J Neurosci. 2007; 27:3571–3583. [PubMed: 17392473]

Duchen LW, Eicher EM, Jacobs JM, Scaravilli F, Teixeira F. Hereditary leucodystrophy in the mouse: the new mutant twitcher. Brain. 1980; 103:695–710. [PubMed: 7417782]

Erturk A, Hellal F, Enes J, Bradke F. Disorganized microtubules underlie the formation of retraction bulbs and the failure of axonal regeneration. J Neurosci. 2007; 27:9169–9180. [PubMed: 17715353]

Escolar ML, Poe MD, Provenzale JM, Richards KC, Allison J, Wood S, Wenger DA, Pietryga D, Wall D, Champagne M, Morse R, Krivit W, Kurtzberg J. Transplantation of umbilical-cord blood in babies with infantile Krabbe's disease. N Engl J Med. 2005; 352:2069–2081. [PubMed: 15901860]

Fawcett JW, Keynes RJ. Peripheral nerve regeneration. Annu Rev Neurosci. 1990; 13:43–60. [PubMed: 2183684]

Griffiths I, Klugmann M, Anderson T, Yool D, Thomson C, Schwab MH, Schneider A, Zimmermann F, McCulloch M, Nadon N, Nave KA. Axonal swellings and degeneration in mice lacking the major proteolipid of myelin. Science. 1998; 280:1610–1613. [PubMed: 9616125]

Hellal F, Hurtado A, Ruschel J, Flynn KC, Laskowski CJ, Umlauf M, Kapitein LC, Strikis D, Lemmon V, Bixby J, Hoogenraad CC, Bradke F. Microtubule stabilization reduces scarring and causes axon regeneration after spinal cord injury. Science. 2011; 331:928–931. [PubMed: 21273450]

Hirokawa N, Noda Y, Tanaka Y, Niwa S. Kinesin superfamily motor proteins and intracellular transport. Nat Rev Mol Cell Biol. 2009; 10:682–696. [PubMed: 19773780]

Howard J, Hyman AA. Dynamics and mechanics of the microtubule plus end. Nature. 2003; 422:753–758. [PubMed: 12700769]

Igisu H, Suzuki K. Progressive accumulation of toxic metabolite in a genetic leukodystrophy. Science. 1984; 224:753–755. [PubMed: 6719111]

Ikegami K, Heier RL, Taruishi M, Takagi H, Mukai M, Shimma S, Taira S, Hatanaka K, Morone N, Yao I, Campbell PK, Yuasa S, Janke C, Macgregor GR, Setou M. Loss of alpha-tubulin polyglutamylation in ROSA22 mice is associated with abnormal targeting of KIF1A and modulated synaptic function. Proc Natl Acad Sci U S A. 2007; 104:3213–3218. [PubMed: 17360631]

Jacobs JM, Scaravilli F, De Aranda FT. The pathogenesis of globoid cell leucodystrophy in peripheral nerve of the mouse mutant twitcher. J Neurol Sci. 1982; 55:285–304. [PubMed: 7131035]

Janke C, Bulinski JC. Post-translational regulation of the microtubule cytoskeleton: mechanisms and functions. Nat Rev Mol Cell Biol. 2011; 12:773–786. [PubMed: 22086369]

Jesionek-Kupnicka D, Majchrowska A, Krawczyk J, Wendorff J, Barcikowska M, Lukaszek S, Liberski PP. Krabbe disease: an ultrastructural study of globoid cells and reactive astrocytes at the brain and optic nerves. Folia Neuropathol. 1997; 35:155–162. [PubMed: 9595850]

Joosten EM, Krijgsman JB, Gabreels-Festen AA, Gabreeels FJ, Baars PE. Infantile globoid cell leucodystrophy (Krabbe's disease). Some remarks on clinical, biochemical and sural nerve biopsy findings. Neuropadiatrie. 1974; 5:191–209. [PubMed: 4407759]

Kobayashi S, Katayama M, Satoh J, Suzuki K. The twitcher mouse. An alteration of the unmyelinated fibers in the PNS. Am J Pathol. 1988; 131:308–319. [PubMed: 3358457]

Krabbe K. A New Familial, Infantile Form of Diffuse Brain-Sclerosis. Brain. 1916; 39:74–114.

Lee WC, Tsoi YK, Dickey CA, Delucia MW, Dickson DW, Eckman CB. Suppression of galactosylceramidase (GALC) expression in the twitcher mouse model of globoid cell leukodystrophy (GLD) is caused by nonsense-mediated mRNA decay (NMD). Neurobiol Dis. 2006; 23:273–280. [PubMed: 16759875]

Mar S, Noetzel M. Axonal damage in leukodystrophies. Pediatr Neurol. 2010; 42:239–242. [PubMed: 20304325]

Matsuyama A, Shimazu T, Sumida Y, Saito A, Yoshimatsu Y, Seigneurin-Berny D, Osada H, Komatsu Y, Nishino N, Khochbin S, Horinouchi S, Yoshida M. In vivo destabilization of dynamic microtubules by HDAC6-mediated deacetylation. Embo J. 2002; 21:6820–6831. [PubMed: 12486003]

Miranda CO, Teixeira CA, Liz MA, Sousa VF, Franquinho F, Forte G, di Nardo P, Pinto-do OP, Sousa MM. Systemic Delivery of Bone Marrow-Derived Mesenchymal Stromal Cells Diminishes Neuropathology in a Mouse Model of Krabbe's Disease. Stem Cells. 2011; 29:1738–1751. [PubMed: 21898691]

Miranda CO, Teixeira CA, Sousa VF, Santos TE, Liz MA, Marques AM, Pinto-do OP, Sousa MM. Primary Bone Marrow Mesenchymal Stromal Cells Rescue the Axonal Phenotype of Twitcher Mice. Cell Transplant. 2013

Mitchell DJ, Blasier KR, Jeffery ED, Ross MW, Pullikuth AK, Suo D, Park J, Smiley WR, Lo KW, Shabanowitz J, Deppmann CD, Trinidad JC, Hunt DF, Catling AD, Pfister KK. Trk activation of the ERK1/2 kinase pathway stimulates intermediate chain phosphorylation and recruits cytoplasmic dynein to signaling endosomes for retrograde axonal transport. J Neurosci. 2012; 32:15495–15510. [PubMed: 23115187]

Pagano RE, Puri V, Dominguez M, Marks DL. Membrane traffic in sphingolipid storage diseases. Traffic. 2000; 1:807–815. [PubMed: 11208071]

Pereira AJ, Maiato H. Improved kymography tools and its applications to mitosis. Methods. 2010; 51:214–219. [PubMed: 20085815]

Pryor S, McCaffrey G, Young LR, Grimes ML. NGF causes TrkA to specifically attract microtubules to lipid rafts. PLoS One. 2012; 7:e35163. [PubMed: 22496904]

Reed NA, Cai D, Blasius TL, Jih GT, Meyhofer E, Gaertig J, Verhey KJ. Microtubule acetylation promotes kinesin-1 binding and transport. Curr Biol. 2006; 16:2166–2172. [PubMed: 17084703]

Ribbens JJ, Moser AB, Hubbard WC, Bongarzone ER, Maegawa GH. Characterization and application of a disease-cell model for a neurodegenerative lysosomal disease. Mol Genet Metab. 2013

Rivieccio MA, Brochier C, Willis DE, Walker BA, D'Annibale MA, McLaughlin K, Siddiq A, Kozikowski AP, Jaffrey SR, Twiss JL, Ratan RR, Langley B. HDAC6 is a target for protection and regeneration following injury in the nervous system. Proc Natl Acad Sci U S A. 2009; 106:19599–19604. [PubMed: 19884510]

Sabatelli M, Quaranta L, Madia F, Lippi G, Conte A, Lo Monaco M, Di Trapani G, Rafi MA, Wenger DA, Vaccaro AM, Tonali P. Peripheral neuropathy with hypomyelinating features in adult-onset Krabbe's disease. Neuromuscul Disord. 2002; 12:386–391. [PubMed: 12062257]

Sakai N, Inui K, Tatsumi N, Fukushima H, Nishigaki T, Taniike M, Nishimoto J, Tsukamoto H, Yanagihara I, Ozono K, Okada S. Molecular cloning and expression of cDNA for murine galactocerebrosidase and mutation analysis of the twitcher mouse, a model of Krabbe's disease. J Neurochem. 1996; 66:1118–1124. [PubMed: 8769874]

Simons K, Gruenberg J. Jamming the endosomal system: lipid rafts and lysosomal storage diseases. Trends Cell Biol. 2000; 10:459–462. [PubMed: 11050411]

Smith B, Galbiati F, Cantuti-Castelvetri L, Givogri MI, Lopez-Rosas A, Bongarzone ER. Peripheral neuropathy in the Twitcher mouse involves the activation of axonal caspase 3. ASN Neuro. 2011; 3:art:e00066.

Sourander P, Olsson Y. Peripheral neuropathy in globoid cel leucodystrophy (morbus Krabbe). Acta Neuropathol. 1968; 11:69–81. [PubMed: 4177348]

Tanaka K, Nagara H, Kobayashi T, Goto I. The twitcher mouse: accumulation of galactosylsphingosine and pathology of the sciatic nerve. Brain Res. 1988; 454:340–346. [PubMed: 3409017]

Tsui-Pierchala BA, Encinas M, Milbrandt J, Johnson EM Jr. Lipid rafts in neuronal signaling and function. Trends Neurosci. 2002; 25:412–417. [PubMed: 12127758]

Wenger DA, Rafi MA, Luzi P. Molecular genetics of Krabbe disease (globoid cell leukodystrophy): diagnostic and clinical implications. Hum Mutat. 1997; 10:268–279. [PubMed: 9338580]

White AB, Givogri MI, Lopez-Rosas A, Cao H, van Breemen R, Thinakaran G, Bongarzone ER. Psychosine accumulates in membrane microdomains in the brain of krabbe patients, disrupting the raft architecture. J Neurosci. 2009; 29:6068–6077. [PubMed: 19439584]

Zaka M, Rafi MA, Rao HZ, Luzi P, Wenger DA. Insulin-like growth factor-1 provides protection against psychosine-induced apoptosis in cultured mouse oligodendrocyte progenitor cells using primarily the PI3K/Akt pathway. Mol Cell Neurosci. 2005; 30:398–407. [PubMed: 16169744]

Zaka M, Wenger DA. Psychosine-induced apoptosis in a mouse oligodendrocyte progenitor cell line is mediated by caspase activation. Neuroscience Letters. 2004; 358:205–209. [PubMed: 15039117]

Zweifel LS, Kuruvilla R, Ginty DD. Functions and mechanisms of retrograde neurotrophin signalling. Nat Rev Neurosci. 2005; 6:615–625. [PubMed: 16062170]

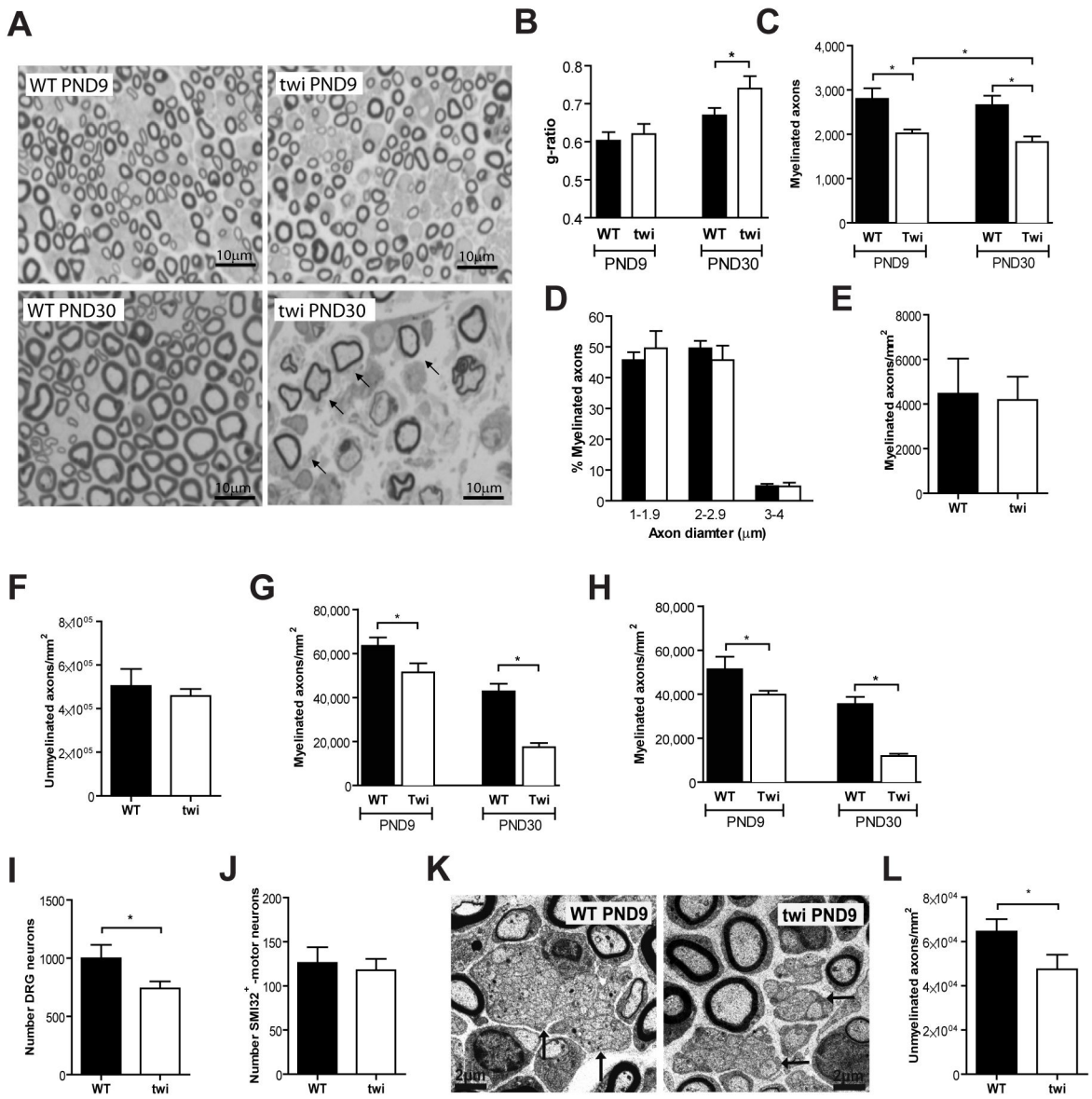

Fig. 1.

In the Twitcher sciatic nerve, a decreased axon number precedes demyelination. (A) Representative photomicrographs of transverse sections of P9 and P30 Twitcher (twi) and WT sciatic nerves are shown; arrows highlight ongoing demyelination with decreased myelin thickness. (B) g-ratio analyses in sciatic nerves of P9 and P30 WT and twi mice. (C) Total number of myelinated axons in the sciatic nerve of P9 and P30 WT and twi mice. (D) Distribution of myelinated axons according to their size in the sciatic nerve of WT and twi mice at P9. For (B–D), n=5 WT and n=5 twi mice at P9 and n=4 WT and n=6 twi mice at P30 were analyzed. (E,F) Density of myelinated (E) and unmyelinated (F) axons in sciatic nerves of P0 WT (n=5) and twi (n=3) mice. (G, H) Density of myelinated axons in the dorsal root (G) and ventral root (H) of WT and twi mice at P9 (n=4 WT and n=5 twi) and at P30 (n=4 WT and n=4 Twi mice). (I) Number of sensory neurons in WT and Twi DRG sections at P9. (J) Number of motor neurons in WT and twi mice (n=4 WT and n=6 twi

mice) in spinal cord sections. (K) Representative electron microscopy photomicrographs of ultrathin sciatic nerve sections of WT and twi mice at P9; arrows highlight Remak bundles. (L) Density of unmyelinated axons in the sciatic nerve of WT and twi mice at P9 (n=5 WT and n=5 twi).

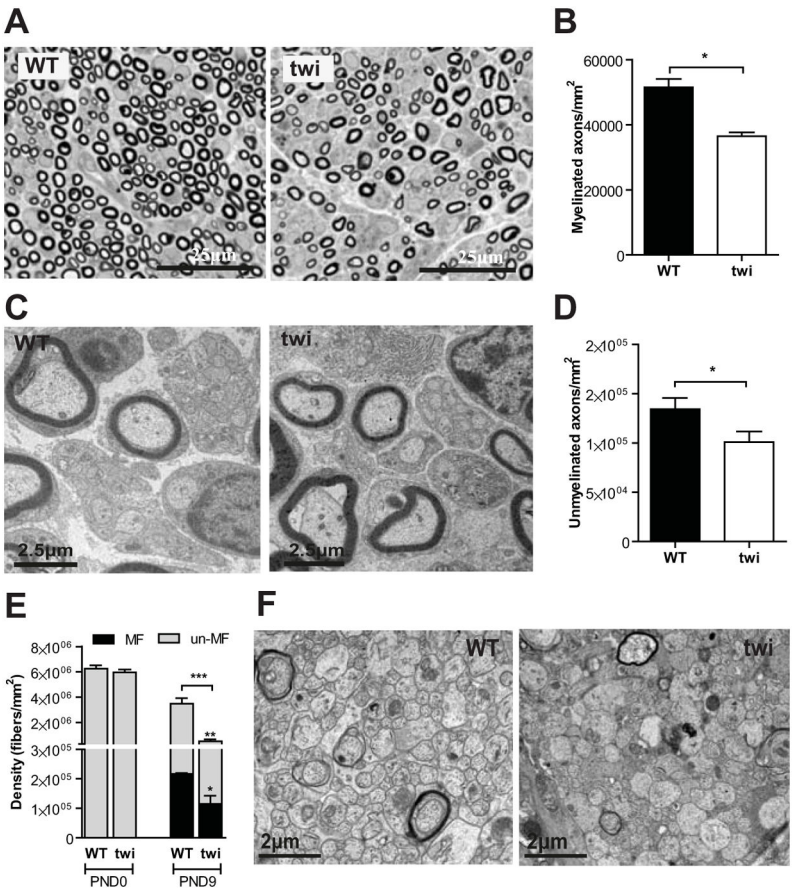

Fig. 2.

A decreased axon number in Twitcher nerves occurs both in the PNS and CNS at P9. (A, C) Representative photomicrographs of the median nerve of WT and twi mice at P9 (A - semithin section, C -ultrathin section). (B, D) Density of myelinated (B) and unmyelinated axons (D) in the median nerve of WT and twi mice at P9 (n=4 WT and n=6 twi mice). (E) Density of myelinated (MF) and unmyelinated (un-MF) axons in the optic nerve of WT and twi mice at P0 (n=4 WT and n=4 twi mice) and P9 (n=4 WT and n=6 twi mice). (F) Representative photomicrographs of the optic nerve of WT and twi mice at P9.

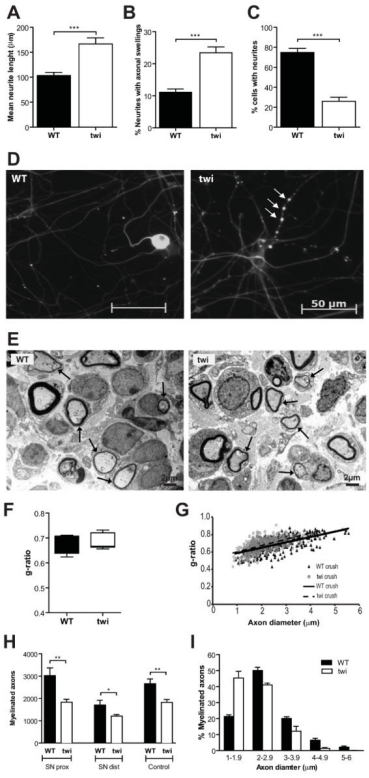

Fig. 3.

Twitcher sciatic nerves are regeneration-competent. (A) Mean neurite length (μm) of WT and Twitcher (twi) DRG neurons after 12h in culture. (B) Percentage of axons with axonal swellings in WT and twi DRG neurons after 5 DIV. (C) Percentage of WT and twi DRG neurons bearing neurites after 7 DIV. (D) Representative photos showing neurite degeneration in twi DRG neurons (arrows highlight degenerating neurites) after 5 DIV. (E) Representative electron photomicrographs of transverse sections of the sciatic nerve, distally to the injury site, showing myelinated axons in both WT and twi, 10 days after crush. Arrows highlight remyelinating axons. (F) Boxplot of the g-ratio values (median, 25–75% inter- quartile range and overall range are represented) and (G) scatter plot showing the correlation between the axon diameter and the g-ratio of myelinated axons in the sciatic nerve of WT (n=4) and twi (n=6) mice, 10 days after crush. (H) Total number of myelinated axons in the sciatic nerve proximally (SN prox) and distally (SN dist) to the injury site (WT, n=4 and twi, n=6), 10 days after crush and in uninjured (control) sciatic nerves of wild type (WT, n=4) and Twitcher (twi, n=6) mice. (I) Distribution of myelinated axons according to their diameter in the sciatic nerve of WT (n=4) and twi (n=6) mice, 10 days after crush.

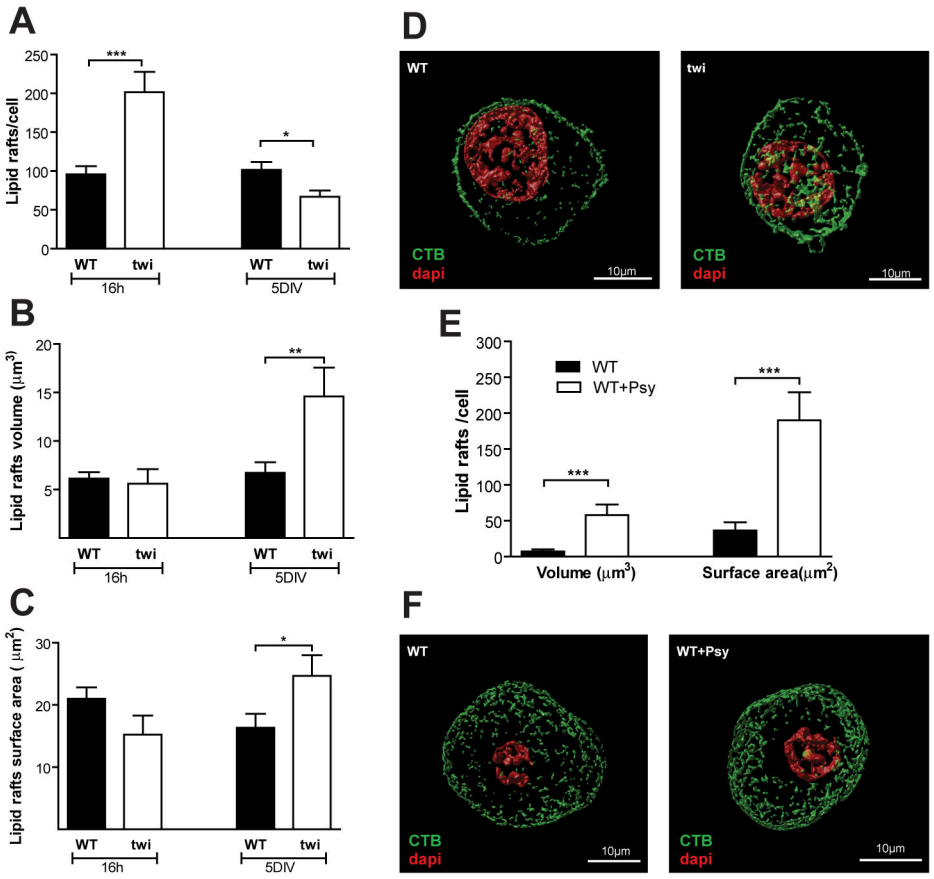

Fig. 4.

Twitcher DRG neurons have an abnormal lipid raft structure. (A) Total number, (B) average volume and (C) surface area of lipid rafts in the DRG neurons of WT and Twitcher (twi) mice after 16 h or 5 days in culture (5DIV). (D) Representative images showing the lipid raft structure in WT and twi DRG neurons. DAPI- red; CTB- green. (E) Average volume and surface area of lipid rafts in WT DRG neurons exposed to 10μg/mL of psychosine (WT +Psy) or ethanol (vehicle) (WT) and maintained 5 DIV. (F) Representative images showing the lipid raft structure in WT and WT+Psy DRG neurons.

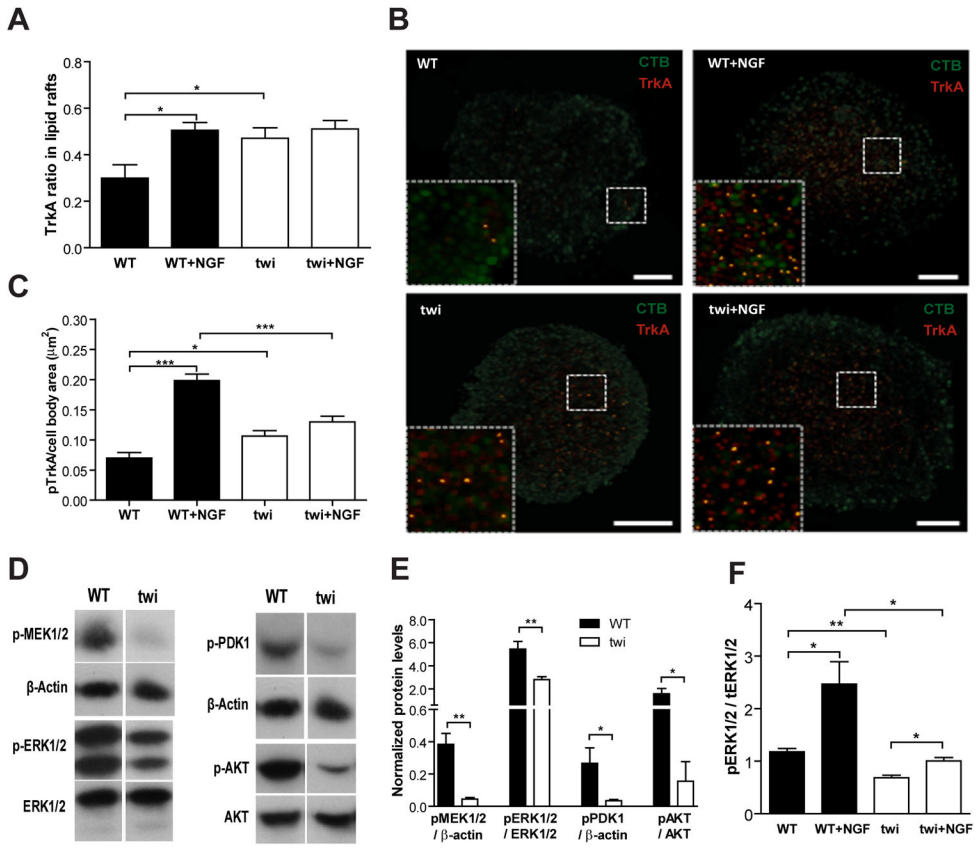

Fig. 5.

Impaired TrkA recruitment and signal transduction in Twitcher DRG neurons. (A) Ratio of TrkA localization in lipid rafts in DRG neurons of WT and Twitcher (twi) mice after 5 DIV either with (WT+NGF and twi+NGF) or without (WT and twi) NGF stimulation. (B) Representative images of the co-localization of TrkA with lipid rafts; TrkA- red, lipid rafts labeled with CTB- green in WT, WT+NGF, twi and twi+NGF DRG neurons. (C) Ratio of phosphorylated TrkA in cell bodies of DRG neurons from WT and twi mice with or without NGF stimulation. (D) Western blot analysis and (E) quantification of the MEK–ERK (left panels) and PDK1–AKT (right panels) pathways in WT and twi DRG neurons. (F) Quantification of ERK activation in WT and twi DRG neurons with or without NGF stimulation.

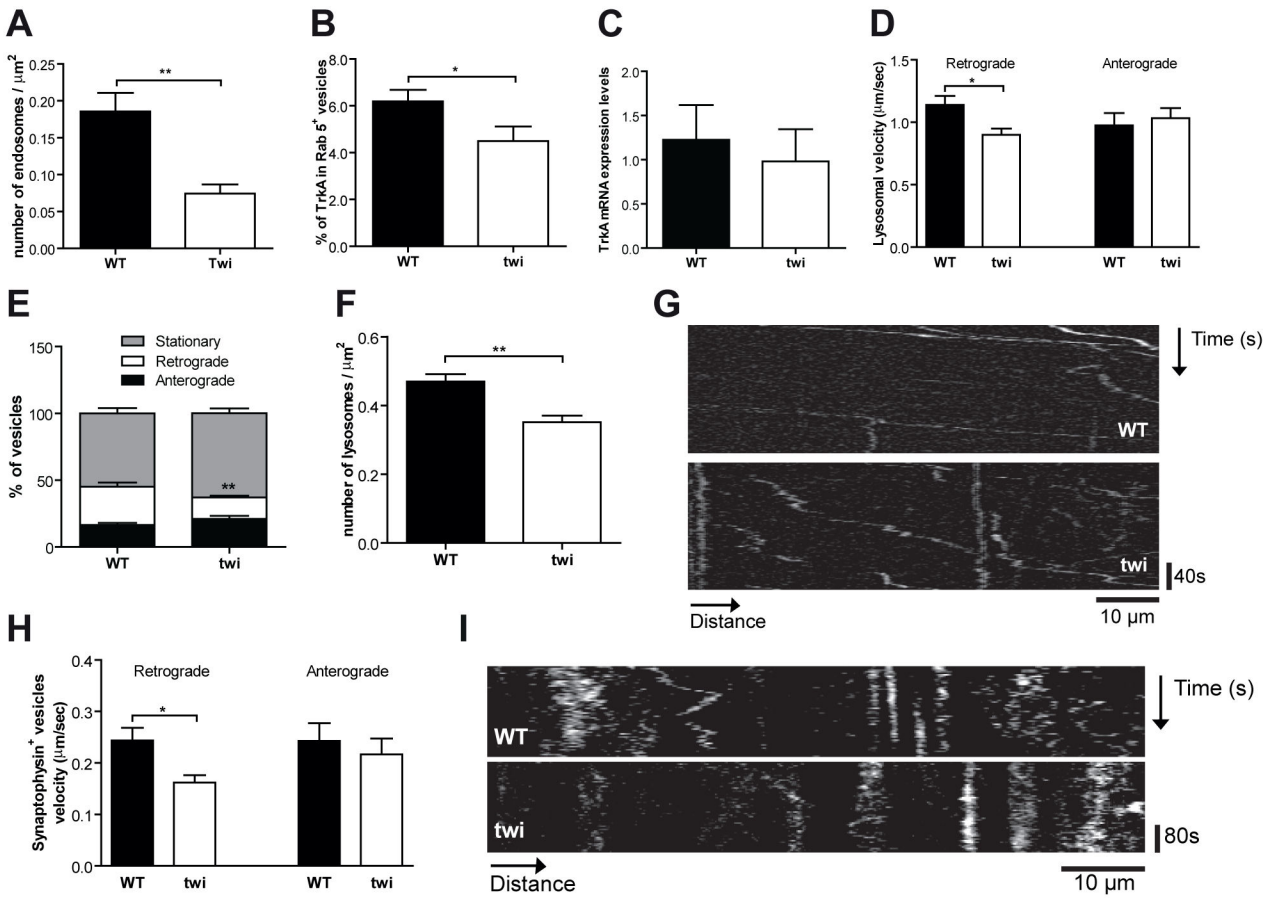

Fig. 6.

The endocytic pathway is impaired in Twitcher DRG neurons. (A) Density of early endosomes in DRG neurons of WT and Twitcher (twi) mice. (B) Percentage of $TrkA^+$ early endosomes ($Rab\ 5^+$ vesicles) in DRG from WT and twi mice. (C) mRNA expression level of TrkA in DRG of WT and twi mice. (D) Velocity of retrograde and anterograde axonal transport of lysosomes in DRG neurites from WT and twi mice. (E) Percentage of stationary lysosomes and lysosomes with retrograde or anterograde movement in DRG neurites from WT and twi mice. (F) Density of lysosomes in DRG from WT and twi mice. (G) Kymographs depicting the movement of lysosomes in WT and twi neurites. (H) Velocity of retrograde and anterograde axonal transport of $synaptophysin^+$ vesicles in DRG neurons of WT and twi mice. (I) Kymographs depicting the movement of $synaptophysin^+$ vesicles in WT and twi axons.

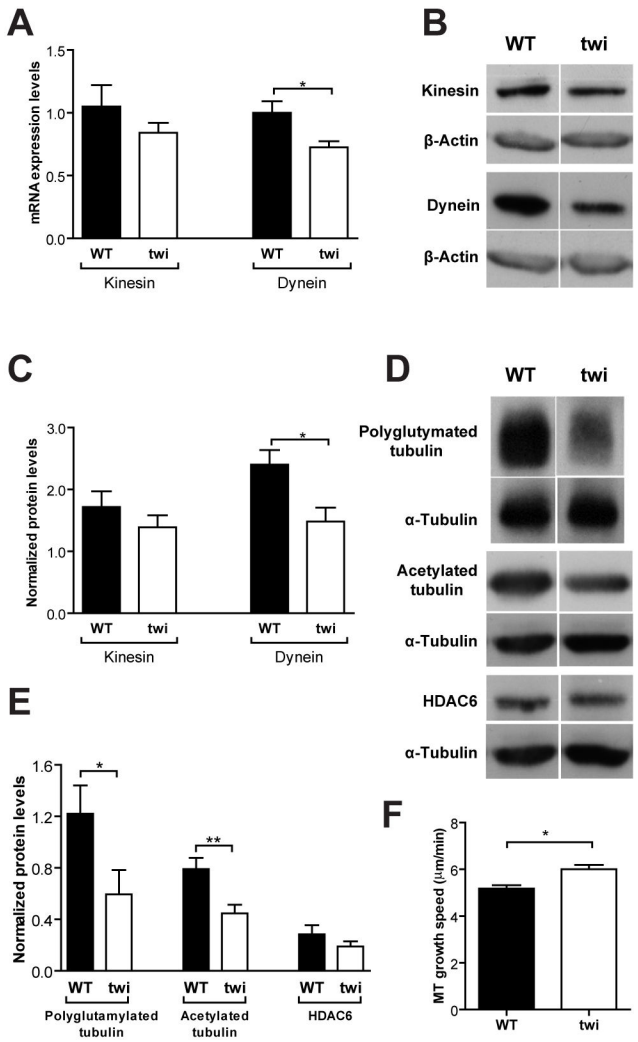

Fig. 7.

Twitcher neurons have lower levels of molecular motors and decreased MT stability. (A) mRNA expression of kinesin-1 and cytoplasmic dynein in P9 DRG of WT and Twitcher (twi) mice. Western blot analysis (B) and quantification (C) of kinesin-1 and cytoplasmic dynein in sciatic nerves of P9 WT and twi mice (n=6 WT mice and n=7 twi). Western blot analysis (D) and quantification (E) of polyglutamylated tubulin, acetylated α-tubulin and HDAC6 in sciatic nerves of P9 WT and twi mice (n=6 WT and n=7 twi mice). (F) Microtubule (MT) growth speed in DRG of WT and twi mice.

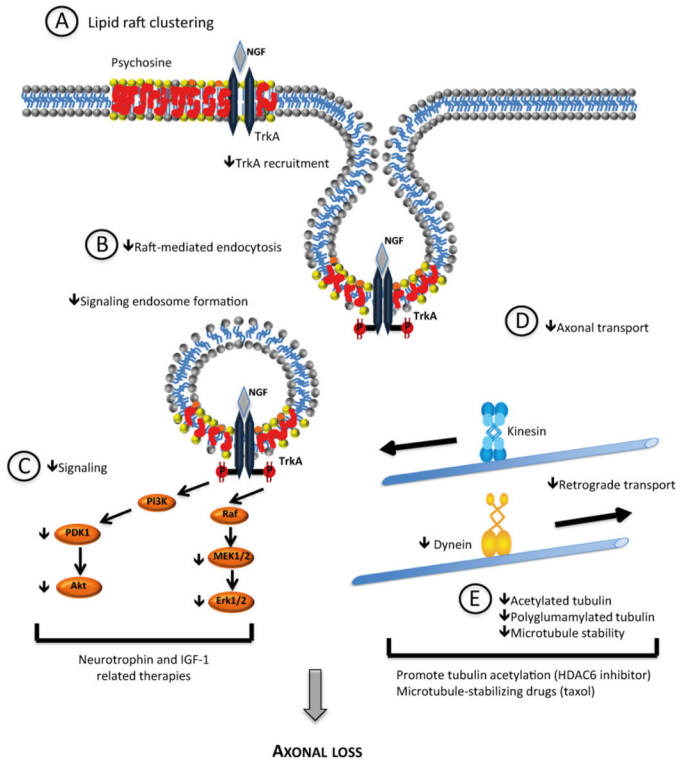

Fig. 8.

Proposed model for the mechanisms contributing to axonopathy in KD neurons. Psychosine accumulation in neuronal membranes causes lipid raft clustering (A), defects in raft-mediated endocytosis and in the formation of signaling endosomes (B). Specifically, there is the impairment of TrkA-mediated signaling (C). At the cytoskeleton level (E), decreased microtubule stability, decreased acetylated and polyglutamylated tubulin and decreased dynein levels generate impaired axonal transport (D). In summary, defects in microtubule stability, axonal transport, and signaling can synergistically lead to axonopathy and ultimately to neuronal loss. As such this model opens novel therapeutic options in KD that may offer neuronal protection, namely IGF-1 and neurotrophin-related therapies, drugs promoting increased tubulin acetylation (such as HDAC6 inhibitors) and microtubule-stabilizing drugs.